Research Article | Vol. 27, No. 2 | 21 Jan 2019 | OPTICS EXPRESS 667
Optics EXPRESS

Structural color filters based on an all-dielectric metasurface exploiting silicon-rich silicon nitride nanodisks

CHUL-SOON PARK,[1] ISHWOR KOIRALA,[1] SONG GAO,[1] VIVEK RAJ SHRESTHA,[1,2] SANG-SHIN LEE,[1,5] AND DUK-YONG CHOI[3,4,6]

[1]*Department of Electronic Engineering, Kwangwoon University, 20 Kwangwoon-ro, Nowon-gu, Seoul 01897, South Korea*
[2]*School of Physics, The University of Melbourne, Melbourne, Victoria 3010, Australia*
[3]*Laser Physics Centre, Research School of Physics and Engineering, Australian National University, Canberra ACT 2601, Australia*
[4]*College of Information Science and Technology, Jinan University, Guangzhou, Guangdong 510632, China*
[5]*slee@kw.ac.kr*
[6]*duk.choi@anu.edu.au*

Abstract: An all-dielectric metasurface is deemed to serve a potential platform to demonstrate spectral filters. Silicon-rich silicon nitride (SRN), which contains a relatively large portion of silicon, can exhibit higher refractive indices, when compared to silicon nitride. Meanwhile, the extinction coefficient of SRN is smaller than that of hydrogenated amorphous silicon, leading to reduced absorption loss in the shorter wavelength. SRN is therefore recommended as a scattering element from the perspective of realizing all-dielectric metasurfaces. In this work, we propose and embody a suite of highly efficient structural color filters, capitalizing on a dielectric metasurface that consists of a two-dimensional array of SRN nanodisks that are embedded in a polymeric layer. The SRN nanodisks may support the electric dipole (ED) and magnetic dipole (MD) resonances via Mie scattering, thereby leading to appropriate spectral filtering characteristics. The ED and MD are identified from field profile observation with the assistance of finite-difference time-domain simulations. The manufactured color filters are observed to produce various colors in both transmission and reflection modes throughout the visible band, giving rise to a high transmission of around 90% in the off-resonance region and a reflection ranging up to 60%. A variety of colors can be realized by tuning the resonance by adjusting the structural parameters such as the period, diameter, and height of the SRN nanodisks. The spectral position of resonances might be flexibly tuned by tailoring the polymer surrounding the SRN nanodisks. It is anticipated that the proposed coloring devices will be actively used for color displays, imaging devices, and photorealistic color printing.

1. Introduction

The metasurface, which is based on a two-dimensional (2D) arrangement of nano-scale scattering elements and thus perceived as a planar counterpart of optical metamaterials, has been researched in virtue of their preeminent capabilities for manipulating the polarization, phase, and amplitude of light in various spectral bands [1–4]. The metasurface can potentially serve as a miniaturized version of the conventional free-space optical devices, encompassing lenses, waveplates, and spectral filters [1–4]. One of the most salient applications empowered by such a metasurface lies in structural color filters, which can provide colors in the visible wavelength regime to possibly supersede dye/pigment-based coloring in display, imaging, color printing, photovoltaic, and so forth [5–9]. To date, a variety of structural color filters and color printing have been attempted, resorting to plasmonic nanoresonators [8–16] and

#348014 https://doi.org/10.1364/OE.27.000667
Journal © 2019 Received 12 Oct 2018; revised 23 Nov 2018; accepted 23 Nov 2018; published 8 Jan 2019

Optics EXPRESS

metasurfaces [17–25]. All-dielectric metasurfaces incorporating high-index materials like crystalline silicon (c-Si), hydrogenated amorphous silicon (a-Si:H), and titanium dioxide (TiO_2) are preferred to their plasmonic counterparts, in which the inherent loss resulting from metallic films prohibits the bandwidth from being controlled. The metasurface in silicon (Si) is advantageous due to its high performance, enhanced cost effectiveness, and good compatibility with the complementary metal-oxide-semiconductor (CMOS) process; while Si, being the second-most-abundant material in nature, exhibits relatively high refractive indices [17–22]. However, it is challenging to grow a high-quality c-Si on a foreign substrate like glass. Polycrystalline silicon (poly-Si), which can be deposited via chemical vapor deposition (CVD), is a viable alternative that provides refractive indices equivalent to that of c-Si. Nevertheless, at temperatures higher than about 300 °C, the deposition of poly-Si on a glass or plastic substrate is hardly permitted. For instance, process techniques including laser/thermal annealing and atomic layer deposition (ALD) were additionally required to form a poly-Si layer on a glass substrate [26,27]. Considering poly-Si is composed of a multitude of small crystallites, optical scattering loss may be caused by the grains. An a-Si:H layer can readily be deposited on a foreign substrate via CVD process at relatively low temperature. Yet, it is vulnerable to relatively high absorptions in the short wavelengths, degrading the efficiency in the blue region [18]. Recently, TiO_2 was adopted as a prominent candidate to construct an all-dielectric metasurface [28–30] and its derivatives like color filters [24,25]. In the meantime, silicon nitride (SiN) has received ample attention as a prime platform for embodying the metasurface, recognizing that its preparation is fully compatible with the CMOS process, while the large bandgap allows for improved transparency and efficiency across the visible band [31,32]. SiN based metasurfaces were taken advantage of to create metalenses, wavefront manipulation, and imaging [31–36]. A suite of structural color filters in SiN was primarily reported based on the guided-mode resonance (GMR) [37–39]. However, no SiN metasurface rendering color generation has yet been interpreted from the viewpoint of Mie scattering mediated resonances. Since SiN gives lower refractive indices compared with the cases of c-Si, a-Si:H, and TiO_2, SiN nanoparticles may not be recommended as an efficient scattering element in the case of an all-dielectric metasurface. It is reported that for nanoparticles exhibiting a certain aspect ratio, the scattering efficiency can be enhanced with increasing refractive indices [40]. Hence, for the case of low-index materials, their surface area should be enlarged to boost the scattering. It should be mentioned that when it comes to Si-rich SiN (SRN), it contains a relatively large portion of Si and thus could offer a higher refractive index compared with SiN and TiO_2. Therefore, it should be reasonably emphasized that SRN is a viable candidate as a foundation for creating a high-quality metasurface. Moreover, SRN allows for a low-temperature deposition via CVD; as a result, the benefit of low absorption in the short wavelengths could be attained, thus overcoming the critical weakness of a-Si:H.

In this work, we suggest an all-dielectric metasurface tapping into an array of SRN nanodisks, enabling considerable scattering, which is crucial for both electric dipole (ED) and magnetic dipole (MD) resonances induced by the Mie scattering. We attempt to concoct a set of structural color filters counting on the proposed SRN metasurface, creating a variety of colors in transmission mode as well as reflection mode. The operation mechanism underlying the proposed metasurface has been inspected through the observation of electric and magnetic field distributions, which are presumed to be responsible for the ED and MD resonances excited by the SRN nanodisks.

2. Optical properties of dielectric materials affiliated with Si

Figure 1 plots the optical properties in the visible wavelength region for dielectric materials associated with Si, inclusive of c-Si, a-Si:H, SRN, and SiN. The refractive indices of c-Si and a-Si:H are available from Palik [41], while those of SRN and SiN are obtained by characterizing their films deposited on a glass substrate using an ellipsometer (J. A. Woollam

M2000D). The c-Si and a-Si:H give rise to high indices (around n = 4). The a-Si:H is unfortunately susceptible to high extinction for shorter wavelengths below λ = 550 nm, causing a significant level of absorption. In contrast, SiN exhibits a relatively lower refractive index in combination with negligible extinction. SiN film is known to be readily attained with the help of CVD at a low temperature of around 250 °C. Noting the composition of SiN film is varied by adjusting the relative flow rates for SiH_4 and NH_4 gases, it is remarked that SiN is engineered to assume higher refractive indices by boosting the content of Si during the deposition process. Consequently, in terms of the efficiency of scattering, SRN is reckoned to be unequivocally preferred to SiN or TiO_2.

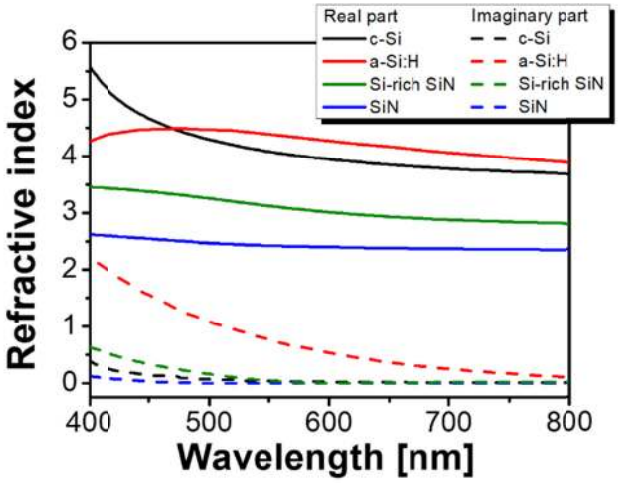

Fig. 1. Dispersion characteristics of Si-related dielectric materials including c-Si, a-Si:H, Si-rich SiN (SRN), and SiN in the visible spectral band. SRN is found to provide higher refractive indices than SiN, while exhibiting lower loss than a-Si:H.

3. Nano-structural coloration enabled by the proposed SRN metasurface

Figure 2 shows the configuration of the proposed all-dielectric metasurface, where a 2D lattice of SRN nanodisks is embedded in a polymeric film on top of a glass substrate. A polymeric material is spin-coated to fill in the gap between nanodisks so as to provide a flat top surface, which is useful for facilitating the planarization crucial for the practical integration of image sensors [42,43]. The polymer, which can increase the refractive index of the medium surrounding the nanodisks, helps bring the transmission dip and reflection peak close together. It is hence beneficial that the center of resonance is concretely rather than vaguely defined to better predict the resulting coloring behavior. A copolymer, ZEP520A, which has been popularly utilized as an electron-beam resist, is selected for building the polymeric layer. The height (H) of the SRN nanodisks is set to 200 nm, which is nearly the thickness of the polymeric layer. The diameter (D) is varied from 80 nm to 200 nm in steps of 20 nm to implement different metasurfaces operating in the visible band, while the period (P) is determined in accordance with the relationship given by P = D + 200 [nm]. For a metasurface resorting to cylindrical nanoparticles, the resonance condition is likely to be controlled by tailoring the structural parameters, such as the height and diameter [44]. The detailed fabrication procedure is elaborated on in a later section. Figure 2 shows that the presence of the metasurface which relies on the SRN nanodisks embedded in a polymer causes incident light to be spectrally filtered out to exhibit flexible coloring in the visible band. The corresponding electric (E-) and magnetic (H-) fields are aligned parallel to the x- and y-axis, respectively. Scanning electron microscope (SEM) image of the fabricated metasurface, subscribing to the design parameters of P = 400 nm, D = 200 nm, and H = 200

nm, is displayed in the inset of Fig. 2. The SRN nanodisks embedded in the polymer (ZEP520A) appear to be embodied in a high fidelity to the design, as desired.

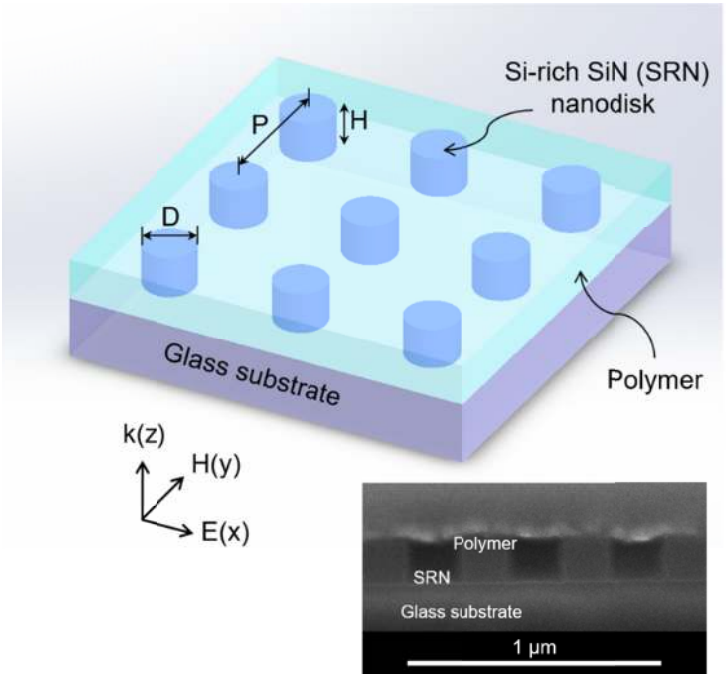

Fig. 2. Configuration of the proposed all-dielectric metasurface resorting to SRN nanodisks built into a polymeric layer. The inset depicts a cross-sectional view of the metasurface which comprises an array of SRN nanodisks with the dimensions of P = 400 nm, D = 200 nm, and H = 200 nm.

The measured and calculated transmission responses for different metasurfaces are plotted in Fig. 3(a). The spectral positions in relation to the ED and MD resonances are traced for each case and marked in dashed lines. The operation and origin of the resonances are discussed further in the next section. The transmission response has been calculated using a commercially available simulation tool, FDTD Solutions (Lumerical, Canada), which is based on the finite-difference time-domain (FDTD) method [45]. The optical transmission spectra were practically examined by a fiber-coupled spectrometer. The observed coloring outputs in transmission mode for the proposed devices, which were fabricated in the pixel sizes of 40 μm × 40 μm, are revealed in Fig. 3(b). The related chromaticity coordinates were obtained from the measured and calculated spectra and mapped on the standard International Commission on Illumination (CIE) 1931 chromaticity diagram, as shown in Fig. 3(c).

Optics EXPRESS

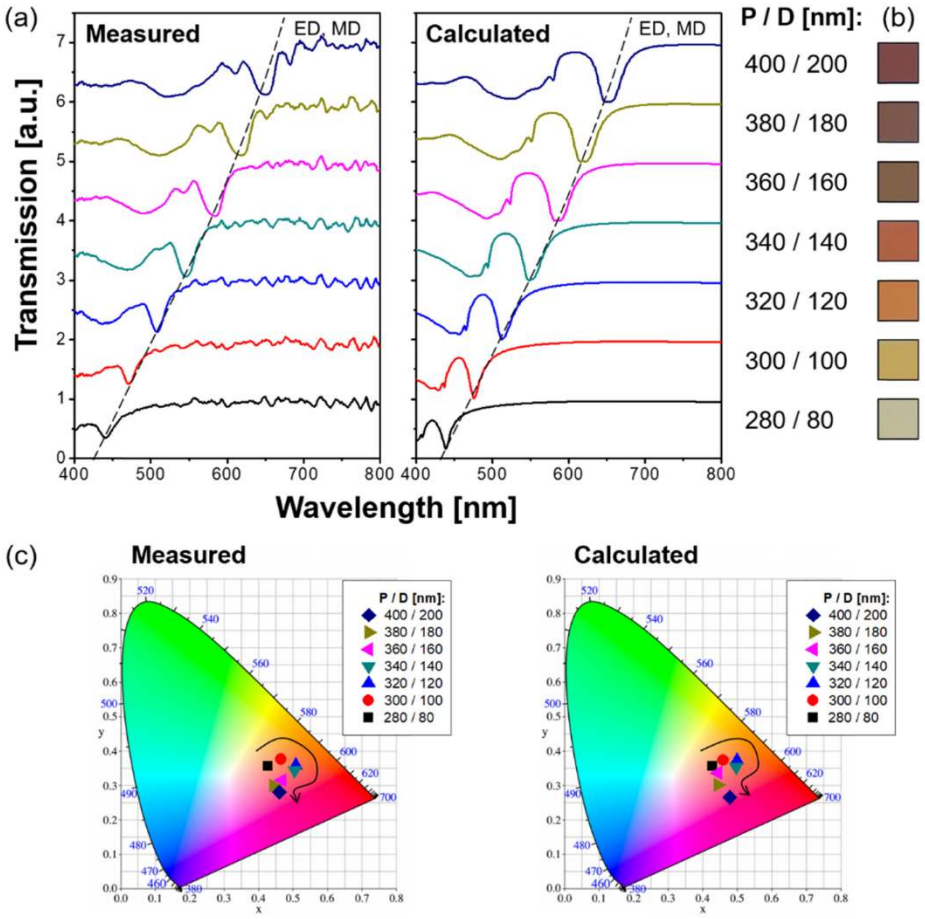

Fig. 3. (a) Measured and calculated transmission spectra for the fabricated color filters. (b) Their color outputs in transmission mode. (c) CIE 1931 chromaticity diagrams corresponding to the measured and calculated spectra, respectively.

The reflection spectra for the prepared color filters were similarly scrutinized, in conjunction with the coloring performance in reflection mode. The reflection spectra and corresponding color images as captured by a microscope are presented in Figs. 4(a) and 4(b), respectively. The observed outcome indicates that the device performance has been slightly affected by fabrication errors. The prepared metasurfaces are monitored to provide colors scanning from light blue, through yellowish green, to orange in reflection mode, when the structural parameters of the SRN nanodisks like the period and diameter are varied. The proposed SRN metasurface tends to give rise to higher efficiencies in longer wavelengths than in shorter wavelengths, which is attributed to the fact that the resonances mediated by the Mie scattering are highly promoted in the spectral regime near λ = 550 nm, in light of the dimensions of the SRN nanodisks. In contrast, the reflection efficiency is severely degraded in the shorter wavelength region, on account of nonnegligible optical extinction on top of inefficient scattering mediated resonance. The efficiency can be elevated in the shorter wavelength band below λ = 550 nm, when structural parameters including the height and diameter are properly adjusted to mediate scattering. This work was particularly concerned about the height of H = 200 nm. The related chromaticity coordinates for the reflection spectra are plotted on the CIE 1931 chromaticity diagram, as sketched in Fig. 4(c).

Optics EXPRESS

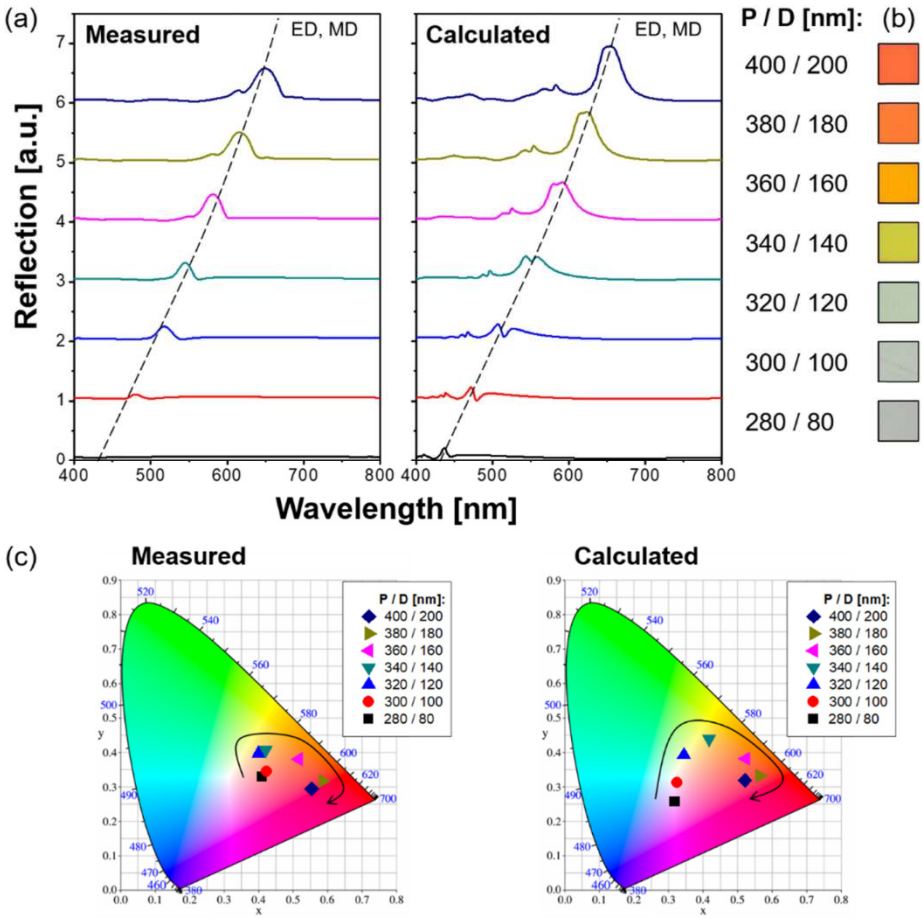

Fig. 4. (a) Measured and calculated reflection spectra for the fabricated color filters. (b) Their color outputs in reflection mode. (c) CIE 1931 chromaticity diagrams corresponding to the measured and calculated spectra, respectively.

In order to achieve a variety of colors, we adjusted the structural parameters such as P and D at the same time. A periodic boundary condition was adopted for the calculation to address coupling between adjacent nanodisks [46]. We also explore the spectra by changing the gap between adjacent nanodisks, which are enclosed in the polymer, while the contour map of the calculated reflection spectra is depicted in Fig. 5(a). The gap is varied from 100 nm to 300 nm in steps of 10 nm, while the height (H) and diameter (D) of the nanodisks are fixed at 200 nm. The calculated scattering cross-sections corresponding to gaps of 150 nm, 200 nm, and 250 nm, are delineated in Fig. 5(b). The scattering cross-section is defined as the ratio of the scattered power going through the closed surface to the power-per-unit area for the incident wave. It is observed that for the proposed metasurface which resorts to periodically arranged SRN nanodisks, the spectral response may be tailored by changing the gap between neighboring elements, which might be mutually coupled to a certain extent and affect the resonance characteristics. It is expected that the coupling can be taken advantage of to adjust the phase of transmitted light and manipulate the wavefront [47,48].

Optics EXPRESS

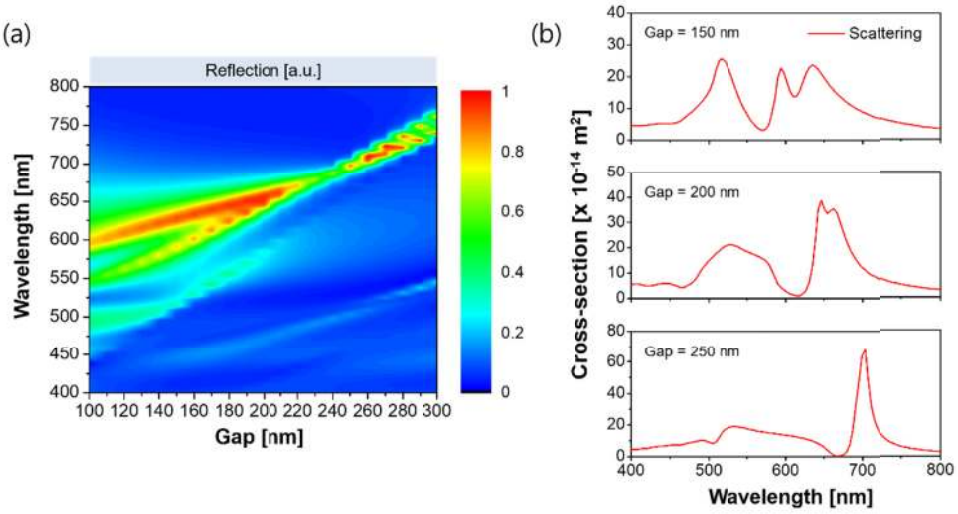

Fig. 5. (a) Contour map of the calculated reflection spectra when the gap between adjacent nanodisks is varied from 100 nm to 300 nm, while the height (H) and diameter (D) of the nanodisks are fixed as 200 nm. (b) Calculated scattering cross-sections corresponding to gaps of 150 nm, 200 nm, and 250 nm.

As depicted in Fig. 2, the proposed metasurface exploits an array of SRN nanodisks that are immersed in a polymeric layer. It is worthwhile to consider the influence of the optical medium enclosing the SRN nanodisks upon the metasurface performance. Toward that end, our metasurface, leveraging the configuration of embedded SRN nanodisks, is compared to a metasurface in which nanodisks are just exposed to air, as summarized in Fig. 6. Here, the metasurfaces are assumed to comprise an identical lattice of SRN nanodisks with P = 400 nm and D = 200 nm. For the case of the nanodisks in contact with air, separate reflection peaks are observed at λ = 582 nm and 642 nm, accounting for the ED and MD resonances, respectively, as indicated by the blue curve. For the proposed metasurface in which the SRN nanodisks are enclosed in a commercialized polymer, ZEP520A with n = ~1.55, the reflection peak in connection with the ED resonance is confirmed to red-shift as anticipated, so that the ED and MD resonances approximately coincide to establish a single peak. The polymer is deemed to increase the effective refractive index of the medium surrounding the nanodisks, so that the resonance peak could shift to longer wavelengths. The ED resonance is believed to red-shift and broaden when the cylindrical nanodisks are immersed in a homogeneous medium, whereas the MD resonance is comparatively less sensitive to the surrounding media [40,49]. Considering that color reproduction is governed by a combination of various wavelengths, a single band of spectral response might be preferable from the perspective of predicting coloring behavior, compared with a multi-band of spectral response [50,51]. The results confirm that the polymeric layer plays the role of preferentially making the reflection peaks for the ED and MD resonances closely neighbor, thereby enhancing the definition of the created colors.

Optics EXPRESS

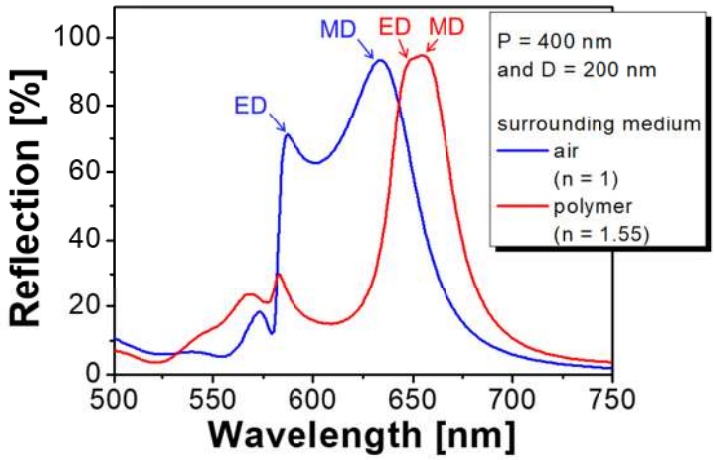

Fig. 6. Reflection spectra for the metasurface with P = 400 nm and D = 200 nm, depending on the surrounding medium. The metasurface whose SRN nanodisks are exposed in air provides distinct reflection peaks for the ED and MD resonances. When the SRN nanodisks are immersed in a polymer with n = 1.55, the resonance peak for the ED is apparently observed to red-shift.

4. Mechanism underlying transmission and reflection resonances for SRN nanodisks

When it comes to nanoparticles made of high-index materials like Si, the ED and MD resonances are presumed to be primarily induced via Mie scattering [44,49,52,53]. To explore the operation principle underpinning the SRN based metasurface, the proposed nanodisks were assessed in terms of the scattering cross-section along with the field profiles, with the assistance of FDTD simulations [45]. The performance of the metasurface under dimensions of P = 400 nm and D = 200 nm is considered, dependent on the presence of the medium surrounding the SRN nanodisks. Figure 7 shows the calculated cross-sections and field profiles for the case where the nanodisks are in contact with air. In regard to the calculated cross-sections in Fig. 7(a), the transmission dip and reflection peak are identified to account for the ED and MD resonances, respectively, which are mediated by the Mie scattering. From the standpoint of the double resonances associated with the metasurface exploiting the SRN nanodisks, the field profiles for the resonance peaks at λ = 582 nm and 642 nm are depicted in Figs. 7(b) and 7(c), respectively. As per the field profiles observed in the yz-plane, as shown in Fig. 7(b), the E-field is chiefly confined in the middle of the SRN nanodisk while the H-field develops a loop in the vicinity of its center at the shorter wavelength of 582 nm, categorically indicative of the ED resonance. As shown in Fig. 7(c), the MD resonance, transpiring at a longer wavelength of 642 nm, which is evident through the enhanced H-field that develops near the center of the disk, alongside the circular E-field pattern. Consequently, the observation of the developed field profiles can distinguish the ED and MD resonances.

Optics EXPRESS

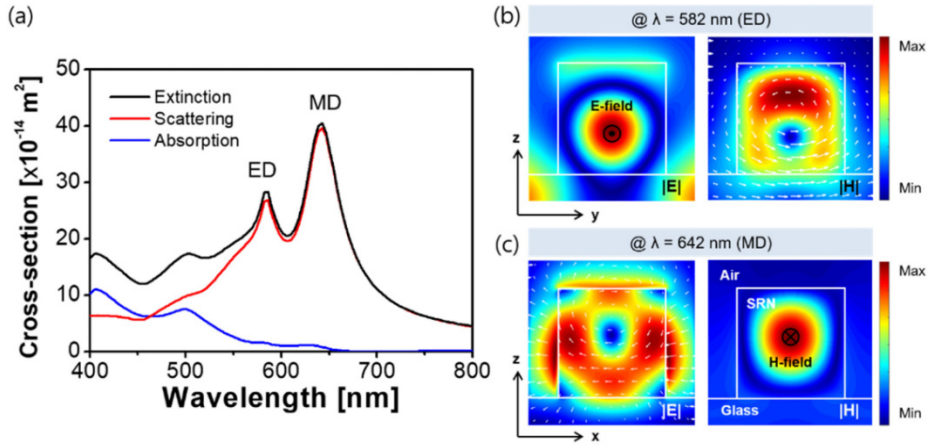

Fig. 7. (a) Scattering, absorption, and extinction cross-sections of the metasurface corresponding to P = 400 nm and D = 200 nm, where the SRN nanodisks are in contact with air. (b) E-field (left) and H-field (right) profiles for the ED resonance at λ = 582 nm as observed in the yz-plane. (c) Field profiles for the MD resonance at λ = 642 nm as observed in the xz-plane.

Likewise, we scrutinized the proposed metasurface which engages a lattice of SRN nanodisks embedded in the polymeric layer of ZEP520A. As portrayed in Fig. 8(a), the ED and MD resonances almost coincide, exhibiting a wavelength separation of as small as 18 nm. Though the nanodisks placed in the polymer may incur a wavelength shift for the ED resonance, the field profiles in charge of the ED and MD resonances, corresponding to λ = 646 nm and 662 nm, are displayed in Figs. 8(b) and 8(c), respectively. As sketched in Fig. 8(b), the E-field in conjunction with the circular H-field is reinforced near the center of the nanodisk at λ = 646 nm, underscoring the existence of the ED resonance. The reinforced H-field near the center of the nanodisk in combination with the surrounding E-field loop is believed to represent the MD resonance at λ = 662 nm, as shown in Fig. 8(c). It is noteworthy that similar phenomena may hold true for the rest of the devices adopting different design parameters.

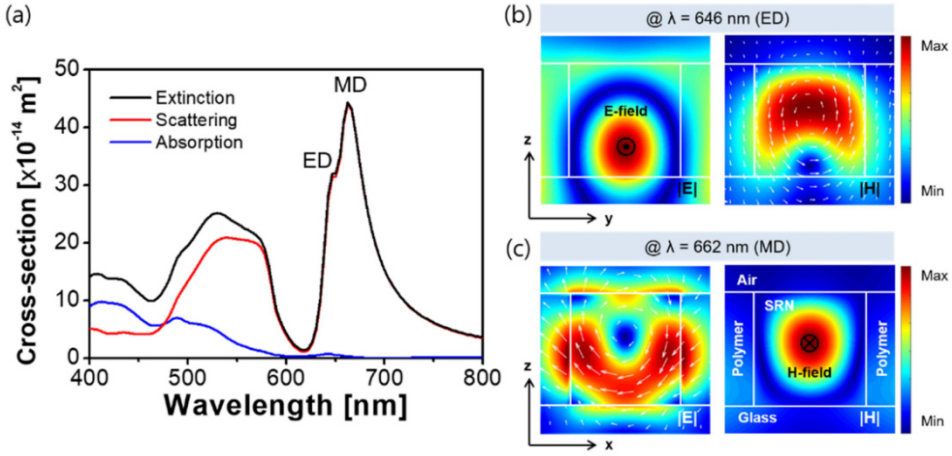

Fig. 8. (a) Scattering, absorption, and extinction cross-sections of the metasurface corresponding to P = 400 nm and D = 200 nm, where the SRN nanodisks are in contact with a polymer of ZEP520A. (b) E-field (left) and H-field (right) profiles for the ED resonance at λ = 646 nm as observed in the yz-plane. (c) Field profiles for the MD resonance at λ = 662 nm as observed in the xz-plane.

Optics EXPRESS

5. Methods

5.1 Numerical simulations

The refractive indices of the SRN and SiN films were obtained by using an ellipsometer (J. A. Woollam M2000D) operating in the spectral range from 193 nm to 1,690 nm, while the dispersion characteristics of c-Si and a-Si:H are derived from Palik [41]. For the proposed all-dielectric metasurfaces, the transmission/reflection spectra, extinction cross-sections, and field profiles were estimated by means of the FDTD method-based tool [45]. A normally incident plane wave was illuminated to a unit cell, satisfying a periodic boundary condition, so that an array of periodically arranged SRN nanodisks could be emulated.

5.2 Device fabrication

The proposed color filters were manufactured to exhibit dimensions of 40 μm × 40 μm. A 200-nm thick SRN film was deposited on a glass substrate in plasma enhanced CVD system (Plasmalab 100, Oxford), where a mixture of SiH_4 and NH_3 diluted in helium was used as a precursor gas. By altering the SiH_4 to NH_3 gas ratio, we could tailor the nitrogen content in a grown film; i.e., with the help of ammonia gas, the portion of nitrogen in the film is increased, thus reducing the extinction coefficient in the visible band and the corresponding refractive index. The adopted process entails: Gas flow rates of 7.5 sccm SiH_4 / 4 sccm NH_3 / 142.5 sccm He, a gas pressure of 850 mTorr, a power of 30 W at 13.56 MHz (radio frequency), and a substrate temperature of 300 °C. After spin coating of an electron beam resist (ZEP520A from Zeon Chemicals), a thin layer of e-spacer 300Z (Showa Denko) was introduced to prevent charging during subsequent electron beam exposure. The nanostructure pattern was then formed using an electron beam writer (EBL, Raith150) and developed in ZED-N50. A 60-nm thick Al layer was subsequently deposited by e-beam evaporation (Temescal BJD-2000), accompanied by a lift-off process in which the sample is soaked in a resist remover (ZDMAC from ZEON Co.). An array of remaining rectangular Al patterns was used as the etch mask to transfer the designed pattern into the SRN film through inductively coupled plasma-reactive ion etching (Plasmalab System 100, Oxford). The etching conditions were optimized to achieve a highly anisotropic profile for the SRN layer, while CHF_3 with a small addition of SF_6 gas was used as plasma etch chemistry. The residual Al etch mask was finally removed by wet etching. The resist, serving as the polymer, was spin-coated to enclose the SRN nanodisks.

5.3 Optical characterization

The completed SRN pattern was visually evaluated by dual beam (SEM/FIB) high-resolution scanning electron microscopy (FIB II, Quanta 3D FEG, FEI). The transmission spectra were obtained by a spectrometer (Avaspec-3648, Avantes) which is tethered to a multimode fiber, while a collimated beam originating from a halogen lamp (HL-2000-FHSA, Ocean Optics) was shone via a focusing lens to the prepared filter that was mounted on a motorized rotation stage. For the proposed devices, the spectral response is stable for incident angles ranging up to ~5°. With the intention of ensuring that the optical response is governed by normally incident light, the test setup has been devised to exhibit a numerical aperture below 0.017. The reflection spectra were observed by a spectrometer equipped with a reflection probe, which is specifically devised to accept the optical beam that normally reflects from the devices. Color images originating from each pixel of the color filters were taken via a digital microscope (Leica DM4000 M) in transmission mode and a CCD camera attached to the spectrometer was exploited in reflection mode.

6. Conclusion and discussion

Structural color filters employing an all-dielectric metasurface, which exploits a 2D lattice of SRN nanodisks embedded in a polymeric layer, were developed in the visible band to

produce not only subtractive colors in transmission mode but additive colors in reflection mode as well. The proposed metasurface, which incorporates 200-nm-thick SRN nanodisks, provides a high efficiency in the green and red band. The device is anticipated to potentially yield enhanced reflection even in the shorter spectral regime when the structural parameters associated with the nanodisks are appropriately selected. Thanks to the introduction of a proper polymer medium enclosing the SRN nanodisks, the overall spectral response of the filters could be effectively engineered to approximately assume a single dominant resonance, thus enabling the prediction of achievable color outputs. The ED and MD resonances mediated by the Mie scattering were keenly scrutinized through the analysis of the field profiles pertaining to the SRN nanodisk structures. Under the deliberation that from the viewpoint of the structural coloring, SiN was mostly employed to implement narrow band filters based on the GMR effect [37–39], the refractive index of SiN has been substantially elevated to become SRN, with a view to making it pertinent to the invocation of scattering in a nanostructure, as verified through the current work. It should be remarked that the resonance could be mediated by Mie type scattering, taking into account the scattering cross-section and the corresponding field profile. Recently, perfect reflection for a periodic structure was explained based on the leaky mode resonance [54,55]. It is expected that considering the proposed metasurface featuring a periodic arrangement of nanostructures provides near-perfect reflection in the spectral band around 650 nm, the leaky mode resonance can be a viable approach for the purpose of inspecting all-dielectric metasurfaces. A wide range of coloring can be made possible by tuning the resonance via the adjustment of the structural parameters of the SRN nanodisks.

Funding

National Research Foundation of Korea (NRF) funded by the Korean government (No. 2016R1A2B2010170 and 2018R1A6A1A03025242); Australian Research Council Future Fellowship (FT110100853, Dr. Duk-Yong Choi).

References

1. A. V. Kildishev, A. Boltasseva, and V. M. Shalaev, "Planar photonics with metasurfaces," Science **339**(6125), 1232009 (2013).
2. N. Yu and F. Capasso, "Flat optics with designer metasurfaces," Nat. Mater. **13**(2), 139–150 (2014).
3. F. Ding, Z. Wang, S. He, V. M. Shalaev, and A. V. Kildishev, "Broadband high-efficiency half-wave plate: a supercell-based plasmonic metasurface approach," ACS Nano **9**(4), 4111–4119 (2015).
4. A. Arbabi, Y. Horie, M. Bagheri, and A. Faraon, "Dielectric metasurfaces for complete control of phase and polarization with subwavelength spatial resolution and high transmission," Nat. Nanotechnol. **10**(11), 937–943 (2015).
5. T. Xu, H. Shi, Y.-K. Wu, A. F. Kaplan, J. G. Ok, and L. J. Guo, "Structural colors: from plasmonic to carbon nanostructures," Small **7**(22), 3128–3136 (2011).
6. S. Kinoshita and S. Yoshioka, "Structural colors in nature: the role of regularity and irregularity in the structure," ChemPhysChem **6**(8), 1442–1459 (2005).
7. H. J. Park, T. Xu, J. Y. Lee, A. Ledbetter, and L. J. Guo, "Photonic color filters integrated with organic solar cells for energy harvesting," ACS Nano **5**(9), 7055–7060 (2011).
8. T. Xu, Y. K. Wu, X. Luo, and L. J. Guo, "Plasmonic nanoresonators for high-resolution colour filtering and spectral imaging," Nat. Commun. **1**(5), 59 (2010).
9. F. Cheng, J. Gao, T. S. Luk, and X. Yang, "Structural color printing based on plasmonic metasurfaces of perfect light absorption," Sci. Rep. **5**(1), 11045 (2015).
10. K. Kumar, H. Duan, R. S. Hegde, S. C. W. Koh, J. N. Wei, and J. K. W. Yang, "Printing colour at the optical diffraction limit," Nat. Nanotechnol. **7**(9), 557–561 (2012).
11. T. Ellenbogen, K. Seo, and K. B. Crozier, "Chromatic plasmonic polarizers for active visible color filtering and polarimetry," Nano Lett. **12**(2), 1026–1031 (2012).
12. Y. S. Do, J. H. Park, B. Y. Hwang, S. M. Lee, B. K. Ju, and K. C. Choi, "Plasmonic color filter and its fabrication for large-area applications," Adv. Opt. Mater. **1**(2), 133–138 (2013).
13. B. Zeng, Y. Gao, and F. J. Bartoli, "Ultrathin nanostructured metals for highly transmissive plasmonic subtractive color filters," Sci. Rep. **3**(1), 2840 (2013).
14. V. R. Shrestha, S. S. Lee, E. S. Kim, and D. Y. Choi, "Aluminum plasmonics based highly transmissive polarization-independent subtractive color filters exploiting a nanopatch array," Nano Lett. **14**(11), 6672–6678 (2014).

Optics EXPRESS

15. Y. Gu, L. Zhang, J. K. W. Yang, S. P. Yeo, and C. W. Qiu, "Color generation via subwavelength plasmonic nanostructures," Nanoscale **7**(15), 6409–6419 (2015).
16. Z. Li, A. W. Clark, and J. M. Cooper, "Dual color plasmonic pixels create a polarization controlled nano color palette," ACS Nano **10**(1), 492–498 (2016).
17. J. Proust, F. Bedu, B. Gallas, I. Ozerov, and N. Bonod, "All-dielectric colored metasurfaces with silicon Mie resonators," ACS Nano **10**(8), 7761–7767 (2016).
18. C. S. Park, V. R. Shrestha, W. Yue, S. Gao, S. S. Lee, E. S. Kim, and D. Y. Choi, "Structural color filters enabled by a dielectric metasurface incorporating hydrogenated amorphous silicon nanodisks," Sci. Rep. **7**(1), 2556 (2017).
19. V. Vashistha, G. Vaidya, R. S. Hegde, A. E. Serebryannikov, N. Bonod, and M. Krawczyk, "All-dielectric metasurfaces based on cross-shaped resonators for color pixels with extended gamut," ACS Photonics **4**(5), 1076–1082 (2017).
20. V. Vashistha, G. Vaidya, P. Gruszecki, A. E. Serebryannikov, and M. Krawczyk, "Polarization tunable all-dielectric color filters based on cross-shaped Si nanoantennas," Sci. Rep. **7**(1), 8092 (2017).
21. Y. Nagasaki, M. Suzuki, and J. Takahara, "All-dielectric dual-color pixel with subwavelength resolution," Nano Lett. **17**(12), 7500–7506 (2017).
22. Y. Nagasaki, M. Suzuki, I. Hotta, and J. Takahara, "Control of Si-based all-dielectric printing color through oxidation," ACS Photonics **5**(4), 1460–1466 (2018).
23. X. Zhu, W. Yan, U. Levy, N. A. Mortensen, and A. Kristensen, "Resonant laser printing of structural colors on high-index dielectric metasurfaces," Sci. Adv. **3**(5), e1602487 (2017).
24. S. Sun, Z. Zhou, C. Zhang, Y. Gao, Z. Duan, S. Xiao, and Q. Song, "All-dielectric full-color printing with TiO_2 metasurfaces," ACS Nano **11**(5), 4445–4452 (2017).
25. I. Koirala, S. S. Lee, and D. Y. Choi, "Highly transmissive subtractive color filters based on an all-dielectric metasurface incorporating TiO_2 nanopillars," Opt. Express **26**(14), 18320–18330 (2018).
26. A. A. D. T. Adikaari, J. D. Carey, V. Stolojan, J. L. Keddie, and S. R. P. Silva, "Bandgap enhancement of layered nanocrystalline silicon from excimer laser crystallization," Nanotechnology **17**(21), 5412–5416 (2006).
27. B. S. So, Y. H. You, K. H. Kim, J. Hwang, W. Cho, S. S. Lee, T. M. Chung, Y. K. Lee, C. G. Kim, K. S. An, Y. C. Kim, Y. H. Lee, and W. S. Seo, "Crystallization of amorphous silicon thin films using self-limiting ALD of nickel oxide," Electrochem. Solid-State Lett. **10**(5), J61–J64 (2007).
28. R. C. Devlin, M. Khorasaninejad, W. T. Chen, J. Oh, and F. Capasso, "Broadband high-efficiency dielectric metasurfaces for the visible spectrum," Proc. Natl. Acad. Sci. U.S.A. **113**(38), 10473–10478 (2016).
29. M. Khorasaninejad, W. T. Chen, R. C. Devlin, J. Oh, A. Y. Zhu, and F. Capasso, "Metalenses at visible wavelengths: Diffraction-limited focusing and subwavelength resolution imaging," Science **352**(6290), 1190–1194 (2016).
30. M. Khorasaninejad, A. Y. Zhu, C. Roques-Carmes, W. T. Chen, J. Oh, I. Mishra, R. C. Devlin, and F. Capasso, "Polarization-insensitive metalenses at visible wavelengths," Nano Lett. **16**(11), 7229–7234 (2016).
31. A. Zhan, S. Colburn, R. Trivedi, T. K. Fryett, C. M. Dodson, and A. Majumdar, "Low-contrast dielectric metasurface optics," ACS Photonics **3**(2), 209–214 (2016).
32. S. Colburn, A. Zhan, E. Bayati, J. Whitehead, A. Ryou, L. Huang, and A. Majumdar, "Broadband transparent and CMOS-compatible flat optics with silicon nitride metasurfaces," Opt. Mater. Express **8**(8), 2330–2344 (2018).
33. S. Colburn, A. Zhan, and A. Majumdar, "Metasurface optics for full-color computational imaging," Sci. Adv. **4**(2), r2114 (2018).
34. A. Zhan, S. Colburn, C. M. Dodson, and A. Majumdar, "Metasurface freeform nanophotonics," Sci. Rep. **7**(1), 1673 (2017).
35. Z.-B. Fan, Z.-K. Shao, M.-Y. Xie, X.-N. Pang, W.-S. Ruan, F.-L. Zhao, Y.-J. Chen, S.-Y. Yu, and J.-W. Dong, "Silicon nitride metalenses for close-to-one numerical aperture and wide-angle visible imaging," Phys. Rev. Appl. **10**(1), 014005 (2018).
36. M. Jang, Y. Horie, A. Shibukawa, J. Brake, Y. Liu, S. M. Kamali, A. Arbabi, H. Ruan, A. Faraon, and C. Yang, "Wavefront shaping with disorder-engineered metasurfaces," Nat. Photonics **12**(2), 84–90 (2018).
37. M. J. Uddin, T. Khaleque, and R. Magnusson, "Guided-mode resonant polarization-controlled tunable color filters," Opt. Express **22**(10), 12307–12315 (2014).
38. M. J. Uddin and R. Magnusson, "Highly efficient color filter array using resonant Si_3N_4 gratings," Opt. Express **21**(10), 12495–12506 (2013).
39. M. J. Uddin and R. Magnusson, "Efficient guided-mode-resonant tunable color filters," IEEE Photonics Technol. Lett. **24**(17), 1552–1554 (2012).
40. B. S. Luk'yanchuk, N. V. Voshchinnikov, R. Paniagua-Domínguez, and A. I. Kuznetsov, "Optimum forward light scattering by spherical and spheroidal dielectric nanoparticles with high refractive index," ACS Photonics **2**(7), 993–999 (2015).
41. E. D. Palik, *Handbook of Optical Constants of Solids* (Academic Press, 1998).
42. H. Park, Y. Dan, K. Seo, Y. J. Yu, P. K. Duane, M. Wober, and K. B. Crozier, "Filter-free image sensor pixels comprising silicon nanowires with selective color absorption," Nano Lett. **14**(4), 1804–1809 (2014).
43. H. Park and K. B. Crozier, "Multispectral imaging with vertical silicon nanowires," Sci. Rep. **3**(1), 2460 (2013).

Optics EXPRESS

44. I. Staude, A. E. Miroshnichenko, M. Decker, N. T. Fofang, S. Liu, E. Gonzales, J. Dominguez, T. S. Luk, D. N. Neshev, I. Brener, and Y. Kivshar, "Tailoring directional scattering through magnetic and electric resonances in subwavelength silicon nanodisks," ACS Nano **7**(9), 7824–7832 (2013).
45. Lumerical Solutions Inc, "FDTD Solutions," https://www.lumerical.com/tcad-products/fdtd/.
46. L. Lin and Y. Yi, "Lattice plasmon resonance in core-shell SiO_2/Au nanocylinder arrays," Opt. Lett. **39**(16), 4823–4826 (2014).
47. K. E. Chong, I. Staude, A. James, J. Dominguez, S. Liu, S. Campione, G. S. Subramania, T. S. Luk, M. Decker, D. N. Neshev, I. Brener, and Y. S. Kivshar, "Polarization-independent silicon metadevices for efficient optical wavefront control," Nano Lett. **15**(8), 5369–5374 (2015).
48. K. E. Chong, L. Wang, I. Staude, A. R. James, J. Dominguez, S. Liu, G. S. Subramania, M. Decker, D. N. Neshev, I. Brener, and Y. S. Kivshar, "Efficient polarization-insensitive complex wavefront control using Huygens' metasurfaces based on dielectric resonant meta-atoms," ACS Photonics **3**(4), 514–519 (2016).
49. A. I. Kuznetsov, A. E. Miroshnichenko, Y. H. Fu, J. Zhang, and B. Luk'yanchuk, "Magnetic light," Sci. Rep. **2**(1), 492 (2012).
50. R. G. Kuehni, *Color: An Introduction to Practice and Principles* (John Wiley & Sons, 2013)
51. R. W. G. Hunt, *The Reproduction of Colour* (John Wiley & Sons, 2004)
52. Y. F. Yu, A. Y. Zhu, R. Paniagua-Domínguez, Y. H. Fu, B. Luk'yanchuk, and A. I. Kuznetsov, "High-transmission dielectric metasurface with 2π phase control at visible wavelengths," Laser Photonics Rev. **9**(4), 412–418 (2015).
53. J. van de Groep and A. Polman, "Designing dielectric resonators on substrates: combining magnetic and electric resonances," Opt. Express **21**(22), 26285–26302 (2013).
54. R. Magnusson and M. Shokooh-Saremi, "Physical basis for wideband resonant reflectors," Opt. Express **16**(5), 3456–3462 (2008).
55. Y. H. Ko and R. Magnusson, "Wideband dielectric metamaterial reflectors: Mie scattering or leaky Bloch mode resonance?" Optica **5**(3), 289–294 (2018).